Advanced Materials Research Vol. 922 (2014) pp 7-12
Online available since 2014/May/07 at www.scientific.net

doi:10.4028/www.scientific.net/AMR.922.7

Simulation of yield strength in Allvac® 718Plus™

M.R. Ahmadi[1,2,3,a], L. Whitmore[4,b], E. Povoden-Karadeniz[1,c],M. Stockinger[5.d], A. Falahati[3,e] and E. Kozeschnik[1,2,3,f]

[1] Christian Doppler Laboratory "Early Stages of Precipitation", Institute of Materials Science and Technology, Vienna University of Technology, Vienna, Austria.
[2] Materials Center Leoben Forschungsgesellschaft mbH, Leoben, Austria.
[3] Institute of Materials Science and Technology, Vienna University of Technology, Vienna, Austria.
[4] Christian Doppler Laboratory for Early Stages of Precipitation, Department of Physical Metallurgy and Materials Testing, Montanuniversität Leoben, Franz-Josef Straße 18, 8700 Leoben, Austria
[5] Böhler Schmiedetechnik GmbH & Co KG, Mariazellerstr. 25, A-8605 Kapfenberg, Austria

[a] mohammad.ahmadi@tuwien.ac.at, [b] lwhitmore@amberwebdesigns.net,
[c]erwin.povoden-karadeniz@tuwien.ac.at, [d] martin.stockinger@bohler-forging.com,
[e]ahmad.falahati@tuwien.ac.at, [f]ernst.kozeschnik@tuwien.ac.at

Keyword: precipitation strengthening, shearing mechanism, anti-phase boundary, coherency strengthening, nickel based superalloy

Abstract

In the present study, we describe a comprehensive and consistent physical model for the yield strength change in Allvac® 718Plus™ caused by precipitation strengthening. The model incorporates the effect of different shearing and non-shearing mechanisms with respect to atomic continuity between the lattices of precipitates and matrix. We demonstrate that coherency and anti-phase boundary effects are the major strengthening mechanisms in this alloy. The final yield strength of Allvac® 718Plus™ during aging is investigated using the thermo-kinetic software MatCalc. The calculated final yield strength evolution is consistent with experimental results.

1 Introduction

Engine performance in aerospace and power generation improves with increasing operation temperature, thus emphasizing the importance of understanding materials with good mechanical properties at high temperatures. Inconel 718 is a nickel based superalloy, which is widely used in aerospace and gas turbine engine applications because of superior high temperature mechanical properties [2] up to 650°C.
In 2004, Allvac® 718Plus™ (hereafter 718Plus) was introduced by ATI Allvac, giving 55K higher service temperature compared to Inconel 718 [3]. 718plus has a similar chemical composition to Inconel 718, however, with higher Ti+Al, Al/Ti ratio and approximately 1% Tungsten. In addition, approximately 50% of Fe is replaced by Co. With this chemical composition, γ' formation is strongly favored in place of γ'', thus eliminating the weakening effect in 718 due to γ'' transformation. The γ' phase is a stable fcc $(Ni,Co)_3(Al,Ti,Cr,Nb)$ precipitate with $L1_2$ structure, with a roughly spherical morphology at low phase fractions and remaining coherent even after over aging [2, 4].
The focus of this paper is the anti-phase boundary (APB) and coherency strengthening effects caused by γ' precipitation.

2 Experimental and computational procedures

MatCalc version 5.52 (rel 0.031) is used for simulation with the thermodynamic database *mc_ni_v2.000_015* and the diffusion database *mc_ni_v2.000_001* [1]. The composition of 718Plus is given in Table 1.

Table 1: Alloying composition of Inconel 718Plus in weight percent [Wt.%]

	Al	Co	Cr	Nb	C	Fe	Mo	Ti	W	Ni
[Wt.%]	1.46	9.13	17.42	5.48	0.028	9.66	2.72	0.71	1.04	bal.

The conventional heat treatment process applied in this work is solution annealing at 975°C for 60 minutes, followed by cold water quenching and aging at 788°C. Hardness and yield strength are measured subsequent to heat treatment and at room temperature. Vickers hardness is measured with a Vickers hardness tester FV 4E to identify precipitation hardening at five aging times (1, 5, 10, 25 and 50 hours). Yield strength is measured by compression testing carried out three times for each sample with Zwick Z250 testing devices. For transmission electron microscopy (TEM) analysis, the specimens are ground with silicon carbide papers down to 0.1mm and electropolished in a solution containing 5% perchloric acid and 95% ethanol at 32 V and -10 °C. The FEI Tecnai F20 microscope is operated with 200 kV acceleration voltage. All samples are pre-cleaned in a He plasma in order to remove surface oxides and impurities.

3 Strengthening model

The final yield strength in heat treatable materials is calculated as a superposition of the inherent stress of the base metal σ_i, grain boundary strengthening σ_g, solid solution strengthening σ_s , work hardening σ_w and precipitation strengthening σ_p, [6].

3.1 Precipitation strengthening. The shearing component of the precipitation strengthening process contains several different strengthening mechanisms: (i) interfacial strengthening, (ii) modulus strengthening, (iii) coherency strengthening and (iv) APB strengthening. Coherency and APB effects are the two predominant strengthening effects in the 718Plus superalloy.

3.1.1 Shearing mechanisms. In this section, we describe the coherency and APB effects for the cases when precipitates are small and shearable (weak mechanism) or large and shearable (strong mechanism).

Coherency effect. The difference in lattice parameter between the precipitate and matrix produces a strain field around the precipitate which hinders dislocation movement. Brown and Ham [7] proposed a strengthening equation for weak and shearable precipitates based on the Gerold and Haberkorn [8] coherency model as

$$\tau_{Coh,weak} = k\left(\frac{G^3 b \varepsilon^3 \bar{r}^3}{L_s^2 T(\theta)}\right)^{\frac{1}{2}}, \tag{1}$$

with,

$$\varepsilon \approx \frac{2}{3}|\delta| \quad \text{and} \quad T(\theta) = \frac{Gb^2}{4\pi}\left(\frac{1+\upsilon-3\sin^2\theta}{1-\upsilon}\right)\ln\left(\frac{r_o}{r_i}\right). \tag{2}$$

k is a constant equal to 4.11 and 1.38 for edge and screw dislocations, respectively. G is the shear modulus, assumed to be 78.0 GPa [4], b is the Burger's vector (0.254 nm), $\bar{r}$ is the precipitate mean radius and L_s the surface-to-surface distance between two precipitates. υ is Poisson's ratio (~0.33), ε is the constrained strain produced by the stress-free strain of lattice misfit δ [9]. δ is the strain measured with 0.004 in this study by TEM analysis. r_o is the outer cut-off distance, which is equal to the distance between two particles along the dislocation line for shearable precipitates [7, 10]. r_i is the inner cut-off distance (=2b [10]) and Θ is the angle between the dislocation line and its Burger's vector in Eq. 2.

The shear stress in Eq. 1 is valid for weak precipitates. For strong precipitates, Brown and Ham [7] proposed the following strengthening equation

$$\tau_{Coh,strong} = \frac{m}{L_s}\left(\frac{T^3(\theta) G \varepsilon \bar{r}}{b^3}\right)^{\frac{1}{4}}, \tag{3}$$

with m being equal to 2.1 and 2 for edge and screw dislocations, respectively.

Anti-phase boundary effect. The anti-phase boundary effect is a strengthening mechanism for ordered precipitates during shearing by dislocations. For weak precipitates

$$\tau_{APB,weak} = \left\{ \frac{2T}{b L_s} \left[\frac{\pi \gamma_{APB} \bar{r}}{4T} \right]^{\frac{3}{2}} - \frac{\pi}{3} \frac{\gamma_{APB} \left(\bar{r}\right)^2}{b L_s^2} \right\}, \tag{4}$$

where γ_{APB} is the APB energy of γ' (=0.111 Jm^{-2} , Ref. [13]). For strong and shearable ordered precipitates, Hüther and Reppich [11] proposed

$$\tau_{APB,strong} = \left(\frac{2wT}{\pi b L_s} \right) \left(\frac{\pi^2 \gamma_{APB} \bar{r}}{4wT} - 1 \right)^{\frac{1}{2}} \tag{5}$$

where *w* is a parameter introduced for remaining dislocation segments incorporating also some other uncertainties. Its value is estimated to be 2.8.

3.1.2 Non-shearing mechanism. At the last stage of aging, the precipitate resistance force in front of the dislocation is sufficiently high to block dislocation movement. The yield strength increases even if the precipitates are still coherent with the matrix. In 1944, Orowan [12] proposed a strengthening equation for spherical and non-shearable precipitates. This equation is modified to the generally accepted form by Ashby [5] and Brown and Ham [7] as

$$\tau_{Orowan} = \frac{Gb}{2\pi\sqrt{1-\upsilon}} \frac{1}{L_s} \ln\left(\frac{\pi}{2} \frac{\bar{r}}{r_i} \right). \tag{6}$$

3.2 Mixture of shearing mechanisms. A general approximation for superposition of different weak or strong strengthening mechanisms *i* was proposed by Ardell [10] to calculate the yield strength increase due to the different strengthening mechanisms with

$$\sigma_{y.p} = M \left(\tau_{Coh,i}^{1.8} + \tau_{APB,i}^{1.8} \right)^{\frac{1}{1.8}}, \tag{7}$$

where *M* is the Taylor factor for converting shear stress to yield strength (*M* ~ 2.6) [14].

4 Results and discussion

The formation of γ' precipitates during aging produces the major effect on the final yield strength in 718Plus. The proposed strengthening equations in section 3.1 are functions of size and distribution of γ', which vary as a consequence of the applied heat treatment. Fig. 1 shows TEM dark field images of 718Plus after aging at 788°C for 1, 10 and 50 hours.

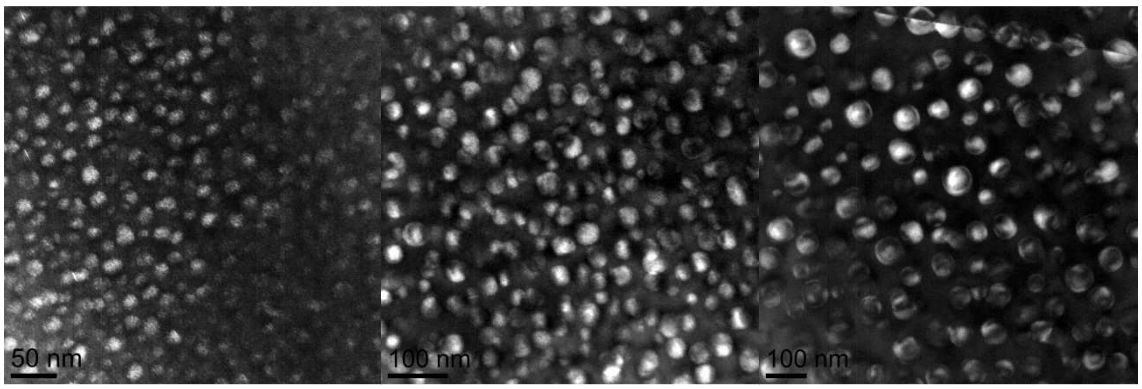

(a) (b) (c)

Fig. 1: Dark field images of 718Plus after aging at 788°C for (a) 1 hr (b) 10 hrs (c) 50 hrs.

From Fig. 1, it is clear that the size of the spherical γ' precipitates increases during aging, while their number density N_s decreases. Simulation of mean radius and number density of γ' is shown in Fig. 2 compared with the experimental results of measurements from the TEM investigation.

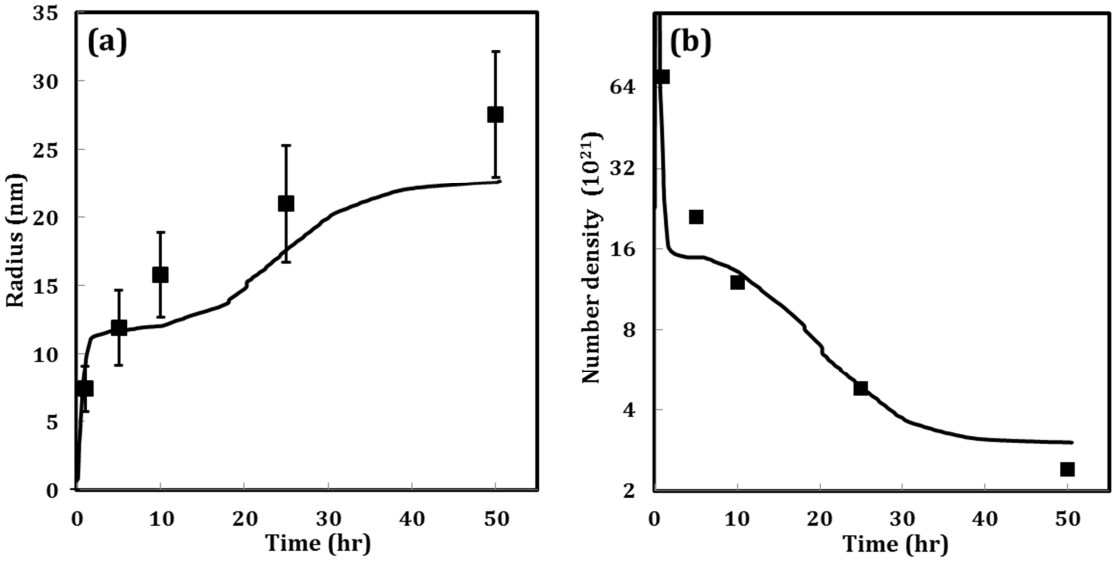

Fig. 2: Simulation result of (a) mean radius (b) number density for 718Plus as a function of aging time at 788°C compared with experimental TEM results

N_s appears in the strengthening equations indirectly as $L_s=1/\sqrt{N_s}$. The simulated and experimental results of aging shown in Fig. 2 demonstrate that precipitate mean radius increases during aging time (improves yield strength) whereas precipitate number density decreases (reduces yield strength).

The experimental results of final yield strength shown in Table 2 represent the maximum yield strength after 10 hours, which is 955 MPa. It means before 10 hours, the effect of mean radius increase dominates against the number density decrement and, as a result, the yield strength increases. After 10 hours, the effect of number density decrement overcomes the mean radius increase and yield strength reduces.

Table 2: Experimental results of yield strength of 718Plus as a function of aging time at 788 °C

	1 hr	5 hr	10 hr	25hr	50 hr
Yield Strength [MPa]	883	900	955	923	900

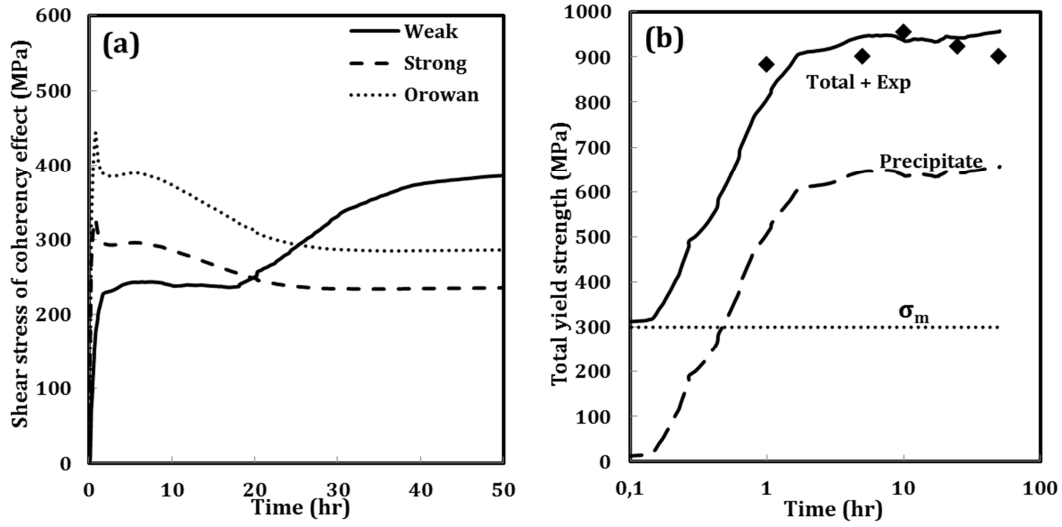

Fig. 3: Simulation of strengthening (a) coherency effect (b) contribution of all strengthening components in final yield strength.

Fig. 3(a) shows simulation results of weak and strong regimes in coherency strengthening independent of other mechanisms, as described in Eqs. 1-3, compared with the Orowan Eq. 6. It is apparent from Fig. 3 (a) that the weak strengthening mechanism defined in Eq. 1 strongly depends upon precipitate radius and has less dependency upon the precipitate free distance. Consequently, in the weak strengthening regime, the shear stress increases by precipitate coarsening during aging. The decrement in strong strengthening regime during aging is due to the weak dependency of strong strengthening equation on the precipitate radius, which results in strong dependency upon the precipitate free distance. Fig. 3 (a) indicates that the operative strengthening regime up to 20 hours is the weak regime, which is replaced by the strong strengthening regime later.
In the same way, the yield strength increase due to the APB effect based on Eqs. 4 and 5 can be simulated. The APB mechanism contributes to the final precipitation strengthening in addition to the coherency effect although this effect is not as significant as the coherency strengthening.
Eq. 7 defines the method used for calculation of total weak and strong precipitation strengthening considering coherency and APB effects. In this study, the γ' precipitate acts as a shearable precipitate even if it has an average diameter of 55 nm.
Fig. 3 (b) shows the magnitude of total yield strength in 718Plus where all the strengthening components except precipitation strengthening are held constant (≈300 MPa) during aging. As displayed in this plot, the main contribution to the total yield strength is the precipitation strengthening, which provides more that 65 % of the total yield strength at peak hardness.

5 Conclusion

- The final yield strength in 718Plus is a combination of contributions from grain boundary, solid solution strengthening, work hardening and precipitation strengthening, in which precipitation strengthening has the highest effect.
- Coherency and APB effects are the two significant strengthening components in the shearing mechanism, and simulation results show that coherency has stronger effect than APB.
- The lattice misfit between γ' precipitates and the matrix is small, consequently precipitates stay coherent even after a long aging time.
- Precipitation strengthening increases during aging when the phase fraction of γ' increases. At the peak of yield strength, the phase fraction of γ' is almost constant. Further aging leads to precipitate coarsening, which subsequently reduces the yield strength.

References:

[1] Information on http://www.matcalc.tuwien.ac.at/

[2] O.A. Idowu, O.A. Ojo, M.C. Chaturvedi, Effect of heat input on heat affected zone cracking in laser welded ATI Allvac 718Plus superalloy, Mater. Sci. and Eng. A 454–455 (2007) 389–397.

[3] W.D. Cao, US Patent No.: 6,730,264B2 (2004).

[4] L. Whitmore, H. Leitner, E. Povoden-Karadeniz, R. Radis, M. Stockinger, Transmission electron microscopy of single and double aged 718Plus superalloy, Mater. Sci. Eng. A 534 (2012) 413– 423.

[5] M.F. Ashby, 'The theory of the critical shear stress and work hardening of dispersion-hardened crystals', in: G.S. Ansell, T.D. Cooper, F.V. Lenel (Eds.), Metallurgical Society Conference, vol. 47, Gordon and Breach, New York, 1968, pp.143-205.

[6] R. Schnitzer, S. Zinner and H. Leitner, Modeling of the yield strength of a stainless maraging steel, Scripta Mater. 62 (2010) 286–289.

[7] LM. Brown, R.K. Ham, Strengthening Methods in Crystals Elsevier Publishing', ed. Kelly and R. B. Nicholson, Elsevier, Amesterdam, The Netherlands, 1971, pp. 9-135.

[8] V. Gerold, H. Haberkorn, On the critical resolved shear stress of solid solutions containing coherent precipitates, Phys Status Solidi (b) 16 (1966) 675-684.

[9] J. D. Eshelby, The determination of the elastic field of an ellipsoidal inclusion, and related problems, Proc. Roy. Soc. A241 (1957) 376-396.

[10] A. J. Ardell, Precipitation hardening, Metal. Trans. 16A (1985) 2131-2165.

[11] W. Huther, B. Reppich, Interaction of Dislocations with Coherent, Stress-Free, Ordered Particles, Z. Metallkunde, Bd. 69 (1978) 628-634.

[12] E. Orowan: Symposium on Internal Stresses in Metals and Alloys, Session III Discussion, Institute of Metals, London, England, (1948) 451-453.

[13] A. J. Ardell, J. C. Huang, Antiphase boundary energies and the transition from shearing to looping in alloys strengthened by ordered precipitates, Phil. Mag. Lett. 58 (1988) 189-197.

[14] B. Clausen, T. Lorentzen, T. Leffers, Self-consistent modelling of the plastic deformation of f.c.c. polycrystals and its implications for diffraction measurements of internal stresses, Acta mater. 46 (1998) 3087-3098.

THERMEC 2013 Supplement
10.4028/www.scientific.net/AMR.922

Simulation of Yield Strength in Allvac® 718Plus™
10.4028/www.scientific.net/AMR.922.7

DOI References
[2] O.A. Idowu, O.A. Ojo, M.C. Chaturvedi, Effect of heat input on heat affected zone cracking in laser welded ATI Allvac 718Plus superalloy, Mater. Sci. and Eng. A 454-455 (2007) 389- 397.
http://dx.doi.org/10.1016/j.msea.2006.11.054
[4] L. Whitmore, H. Leitner, E. Povoden-Karadeniz, R. Radis, M. Stockinger, Transmission electron microscopy of single and double aged 718Plus superalloy, Mater. Sci. Eng. A 534 (2012) 413- 423.
http://dx.doi.org/10.1016/j.msea.2011.11.089
[6] R. Schnitzer, S. Zinner and H. Leitner, Modeling of the yield strength of a stainless maraging steel, Scripta Mater. 62 (2010) 286-289.
http://dx.doi.org/10.1016/j.scriptamat.2009.11.020
[8] V. Gerold, H. Haberkorn, On the critical resolved shear stress of solid solutions containing coherent precipitates, Phys Status Solidi (b) 16 (1966) 675-684.
http://dx.doi.org/10.1002/pssb.19660160234
[9] J. D. Eshelby, The determination of the elastic field of an ellipsoidal inclusion, and related problems, Proc. Roy. Soc. A241 (1957) 376-396.
http://dx.doi.org/10.1098/rspa.1957.0133
[13] A. J. Ardell, J. C. Huang, Antiphase boundary energies and the transition from shearing to looping in alloys strengthened by ordered precipitates, Phil. Mag. Lett. 58 (1988) 189-197.
http://dx.doi.org/10.1080/09500838808214752
[14] B. Clausen, T. Lorentzen, T. Leffers, Self-consistent modelling of the plastic deformation of f. c. c. polycrystals and its implications for diffraction measurements of internal stresses, Acta mater. 46 (1998) 3087-3098.
http://dx.doi.org/10.1016/S1359-6454(98)00014-7